Negative refraction for anti-plane elastic waves in canonical quasicrystalline laminates*

Zhijiang Chen[(1)], **Lorenzo Morini**[(1)] **and Massimiliano Gei**[(2)]

[(1)] *School of Engineering, Cardiff University, The Parade, Cardiff CF24 3AA, UK.*
[(2)] *Department of Engineering and Architecture, University of Trieste, via A. Valerio 6/1, I-34127 Trieste, Italy.*
E-mail: massimiliano.gei@dia.units.it

March 2, 2022

Abstract

Elastic anti-plane shear waves can be refracted negatively when they are transmitted across an interface between a homogeneous substrate and a transverse periodic laminate. To achieve pure negative refraction, the frequency of the source should be lower than the upper limit of the second transition zone of the harmonic spectrum of the laminate. An effective way to control the location of transition zones is to consider a canonical configuration for the laminate, a concept that originates from the properties of quasicrystalline sequences among which the Fibonacci one is a particular case. We give a detailed account of the classification in three families of canonical configurations and the role of canonical frequency. We exploit the knowledge of the scaling factor of the self-similar structure of the layout of transition zones for laminates of this kind to provide a quantitative tool to predict the relevant frequencies to accomplish negative refraction. We also investigate how the change of other parameters of the elementary cell may affect the values of those frequencies. The obtained results show that the features of quasicrystalline sequences may be profitably exploited for the realisation of elastic metamaterials.

Keywords: Fibonacci laminate, Quasiperiodicity, Negative refraction, Canonical frequency.

1 Introduction

In the last two decades, negative refraction of elastic waves at an interface between two dissimilar media and its adoption for innovative applications for vibration control have attracted a significant interest from the scientific community. As it has been illustrated in several studies performed by Professors N.V. Movchan, A.B. Movchan and their collaborators (Farhat et al., 2009, 2010; Brun et al., 2010; Jones et al., 2011; Colquitt et al., 2013; Carta et al., 2017; Tallarico et al., 2017), this phenomenon can be usually observed when elastic waves impinge different types of tailored-designed micro-architected

*Dedicated to Natasha and Sasha Movchan in occasion of their 60th birthday.

interfaces. Recently, the problem of oblique incidence of an anti-plane shear wave at the interface between a substrate and a periodic two-phase laminate has received considerable attention (Nemat-Nasser, 2015; Srivastava, 2016; Willis, 2016; Srivastava and Willis, 2017; Morini et al., 2019a). These studies indicate that, when the layering direction is perpendicular to the interface, it is possible to use a laminate to achieve negative refraction. Conversely, only positive refraction is observed when layers are aligned to the interface with the substrate (Srivastava and Nemat-Nasser, 2014). According to Willis (2016) and Srivastava (2016), to obtain negative refraction when only one mode is transmitted (a circumstance that we will also refer to as pure negative refraction) it is necessary to couple the incident wave with the laminate mode belonging to the second Brillouin zone as it will be clarified later in the text. Minimum wave frequency and threshold angle of incidence can be determined to reach the second Brillouin zone depending on the properties of the elastic system.

In this paper, with the goal of deepening the understanding of the phenomenon of refraction of elastic anti-plane shear waves in laminates, we study wave transmission across the substrate-laminate interface by considering, for the latter, periodic cells generated following the Fibonacci sequence (Morini et al., 2019a). Inspired by the concept of canonical configuration in periodic quasicrystalline-generated rods, recently formulated by Gei et al. (2020), we introduce the notion of *canonical laminate*, that is achieved when the properties of the two selected phases of the composite obey certain mixing rules.

The relevant feature of a canonical laminate is that its frequency spectrum is both symmetric and periodic, with a special frequency, called *canonical frequency*, controlling both phenomena. Moreover, by changing the index of the Fibonacci sequence, the set of layouts of stop and pass bands of the elements of the sequence display a self-similar behaviour in the neighbourhood of certain frequencies with a ratio that can be quantitatively estimated in terms of the invariant function of the sequence.

For the problem of pure negative refraction, the focus on the spectrum is on the first two pass bands at low frequencies, therefore the investigation of self similarity in this range could be particularly useful to select the most suitable periodic cell for the laminate to enhance negative refraction.

The paper is structured to introduce step-by-step all the relevant concepts to reach a full understanding of the important role that a canonical laminate may have for the problem of pure negative refraction. In the first part, the principle underpinning transmission and reflection of waves at the substrate-laminate interface is studied in detail. In particular, it is clarified with an example why the first two pass bands of the frequency spectrum associated with wave propagation orthogonal to the layering direction are important and how they are connected to the second Brillouin zone to secure a negatively refracted wave component in the laminate. Then, we define the notion of *canonical laminate* and show what are the properties brought about by a canonical configuration that can be fully explained by the invariant function of the sequence, i.e. independent of the index of the element of the sequence[1]. In particular, the scaling factor of the first two pass bands is obtained and is exploited as a tool to predict the change in their limits at a change of the index of the sequence. To complete the framework, a section is added

[1]The invariant exists for any quasicrystalline sequence of which the Fibonacci one is a particular case, see Poddubny and Ivchenko (2010).

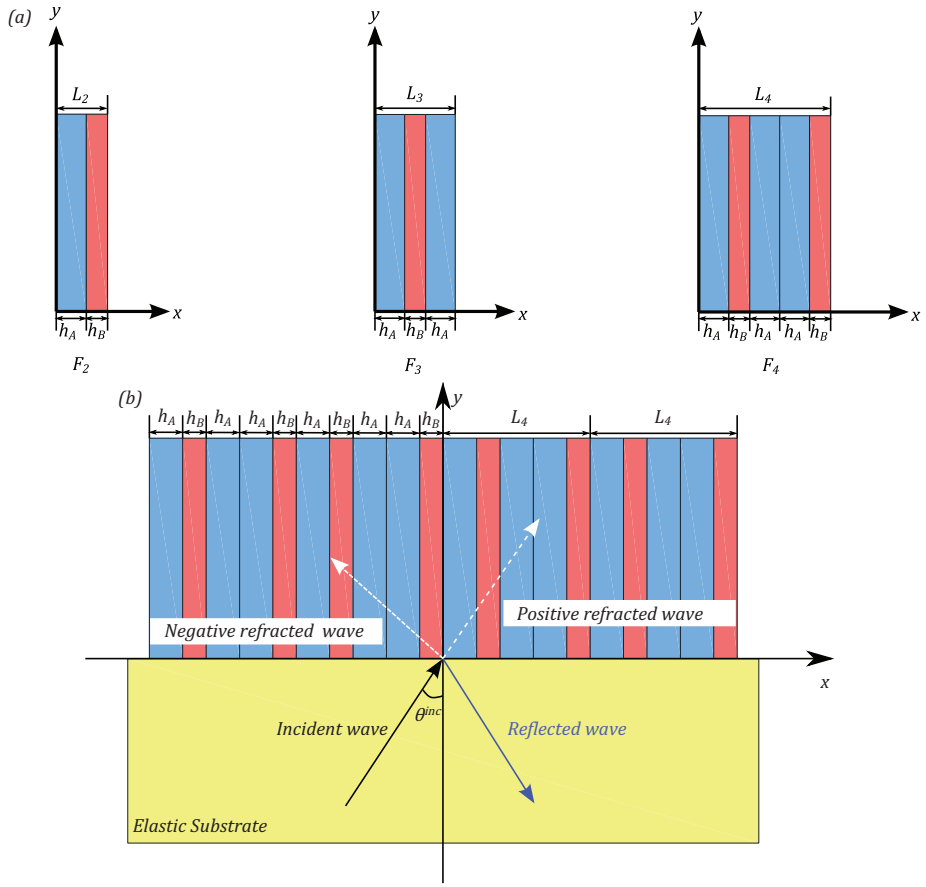

Figure 1: (a) Elementary cells for Fibonacci sequences $\mathcal{F}_2$, $\mathcal{F}_3$ and $\mathcal{F}_4$; (b) reflection and refraction of an anti-plane shear wave approaching the interface between an elastic substrate and a Fibonacci laminate $\mathcal{F}_4$.

in which the effect of changing (i) the materials of the two phases at same canonical ratio and (ii) the total length of the periodic cell is analysed.

2 Refraction of anti-plane shear waves across an interface between a substrate and a transverse periodic quasicrystalline-generated laminate

2.1 Floquet-Bloch waves in periodic laminates

We investigate a set of infinite two-phase periodic laminates whose elementary cells are generated adopting the standard Fibonacci sequence $\mathcal{F}_i$ based on the recursive rule $\mathcal{F}_i = \mathcal{F}_{i-1}\mathcal{F}_{i-2}$, whose initial condition is $\mathcal{F}_0 = B$ and $\mathcal{F}_1 = A$, where A and B are the two homogeneous constituents. The natural number i is the index of the element $\mathcal{F}_i$.

For each phase, shear modulus μ_X, mass density ρ_X and thickness h_X are defined (here and henceforth, $X \in \{A, B\}$). The total length of cell $\mathcal{F}_i$ is given by $L_i = n_i^{(A)} h_A + n_i^{(B)} h_B$, where $n_i^{(A)}$ and $n_i^{(B)}$ are the number of laminae A and B included in the cell, respectively, and the total number of

laminae corresponds to the Fibonacci number $n_i = n_i^{(A)} + n_i^{(B)}$ (see Fig. 1(a)).

By assuming the co-ordinate system displayed in Fig. 1, in which z is the out-of-plane axis, the non-zero displacement of anti-plane shear wave is denoted by $u_z(x, y, t)$ and satisfies the following wave equation within any of the phases of the elementary cell (the subscript X is dropped to ease the notation)

$$\mu \left(\frac{\partial^2 u_z}{\partial x^2} + \frac{\partial^2 u_z}{\partial y^2} \right) = \rho \frac{\partial^2 u_z}{\partial t^2}. \tag{1}$$

The harmonic solution to eq. (1) has the form

$$u_z = w(x) e^{i(\omega t - K_x x - K_y y)}, \tag{2}$$

where ω is the circular frequency, K_x and K_y are the wave numbers and the amplitude function $w(x)$ is periodic. Displacement u_z and shear stress σ_{xz} are continuous across all the interfaces. Solving eq. (1), we get, in each phase, the connection (Lekner, 1994; Brun et al., 2010; Willis, 2016)

$$\begin{bmatrix} \sigma_{xz}(x) \\ u_z(x) \end{bmatrix} = \begin{bmatrix} \cos[q(\omega, K_y)(x - x_l)] & -\mu q(\omega, K_y) \sin[q(\omega, K_y)(x - x_l)] \\ \dfrac{\sin[q(\omega, K_y)(x - x_l)]}{\mu q(\omega, K_y)} & \cos[q(\omega, K_y)(x - x_l)] \end{bmatrix} \begin{bmatrix} \sigma_{xz}(x_l) \\ u_z(x_l) \end{bmatrix}, \tag{3}$$

where the 2×2 matrix therein is the transmission matrix across the phase. In eq. (3), $q(\omega, K_y) = \sqrt{(\omega/c)^2 - K_y^2}$, where c is the phase speed in the relevant material, namely $c_X = \sqrt{\mu_X / \rho_X}$, the vector on the r.h.s. is evaluated at the left-hand interface of the lamina concerned (i.e. x_l), while $x_l \leq x \leq h_X + x_l$.

Therefore, the global transmission matrix M_i corresponding to the cell $\mathcal{F}_i$ is the result of the product

$$M_i = \prod_{p=1}^{n_i} [M_X]_p \quad (X \in A, B). \tag{4}$$

Matrix M_i possesses two relevant properties: (i) it is unimodular, i.e. $\det M_i = 1$; (ii) as a consequence of the recursion rule valid for the Fibonacci sequence, it can be generated through the recursive relationship $M_i = M_{i-2} M_{i-1}$ $(i \geq 2)$.

Floquet-Bloch waves in periodic laminates are governed uniquely by the trace of transmission matrix, i.e. $t_i(\omega, K_y) = \mathrm{tr} M_i(\omega, K_y)$, through the equation

$$\cos(K_x L_i) = \frac{1}{2} t_i(f, K_y), \tag{5}$$

where, with a slight abuse of notation, the frequency $f = \omega/(2\pi)$ is used to replace the circular frequency.

2.2 Pure negative refraction across an interface between a substrate and a transverse laminate

Wave transmission across the interface between a homogeneous elastic substrate and a transverse periodic laminate is a coupled problem (Fig. 1(b)). On the one hand, the possible number of transmitted

	Steel	Iron	Copper	Aluminium	Nylon	PMMA	Polyethylene
μ (GPa)	80	52.5	44.7	26	4	3	0.117
ρ (kg/m^3)	8000	7860	8940	2700	1150	1180	930

Table 1: Properties of the materials adopted in the case studies.

modes depends on both the frequency of the incoming wave f and the properties of the laminate, included in the function t_i; on the other hand, the function $\cos(K_x L_i)$ in eq. (5) depends, in turn, on the properties of the substrate, the frequency and the angle of incidence θ^{inc}, as

$$K_x = K_0 \sin\theta^{\text{inc}} = (2\pi f/c_0)\sin\theta^{\text{inc}}. \tag{6}$$

In eq. (6), K_0 is the wave number of the incoming wave and $c_0 = \sqrt{\mu_0/\rho_0}$ the speed of shear waves in the substrate. This means that as the transmission matrix is already known, the quantity K_y will be solved from eq. (5). An effective plot to represent the real solutions of eq. (5) is the diagram $K_x L_i$ vs $K_y L_i$ similar to those reported in Figs. 2 (a) and (b) (Nemat-Nasser, 2015; Srivastava, 2016; Willis, 2016; Morini et al., 2019a).

The isofrequency curves plotted in Figs. 2(a)(b) are for a laminate $\mathcal{F}_2$ which combines PMMA (material A, $h_A = 3$ mm) and steel (material B, $h_B = 1.3$ mm) whose characteristic parameters are listed in Tab. 1. The analysis of both Figs. 2 (a), (b) allows to understand how to achieve *pure* negative refraction in this periodic laminate as a prototype example.

In particular, we consider the range of frequencies corresponding to the second Brillouin zone (i.e. $\pi < K_x L_i < 2\pi$) and explore, within this interval, the number of real solutions of eq. (5) at varying $K_x L_i$. We can find that for a frequency lower than 93.24 kHz (in Fig. 2(a), $f = 93.24$ kHz is the grey line, dashed in the range of interest, emerging from point $(\pi, 0)$), there could be either none or one solution (none corresponds to total reflection). For instance, for $f = 70$ kHz, the value of the threshold $K_x L_i$ where the branch arises, denoted by $\bar{K}_x L_i$, is 4.481. One solution is confirmed for frequency f between 93.24 and 261.34 kHz, whereas in the range $f \in [261.34, 296.63]$ kHz, the real branches can be either one or two; for $f > 296.63$ kHz, two real solutions are available (a higher frequency at which the number of solutions increases of one may be found, but we are not going further in the investigation because not relevant for our purposes).

The angle of refraction is defined through the direction of Poynting vector $\mathcal{P}$ whose in-plane components $\mathcal{P}_x$ and $\mathcal{P}_y$ share the same directions with components $v_x^g = \partial\omega/\partial K_x$ and $v_y^g = \partial\omega/\partial K_y$ of the group velocity, respectively. In Fig. 2(a), it is easy to recognise that for the branches in the first Brillouin zone (i.e. $0 < K_x L_i < \pi$), the mentioned components are both positive, so is the angle of refraction. On the contrary, in the second Brillouin zone, v_x^g turns out to be negative whereas v_y^g is still positive, therefore the angle becomes negative too, which is our goal. It is worth noticing that, in contrast to what observed in Fig. 2(a), for the range of frequencies considered in Fig. 2(b) there exist coexisting solutions with both positive and negative refractions (beam splitting). In this range, negative refraction may

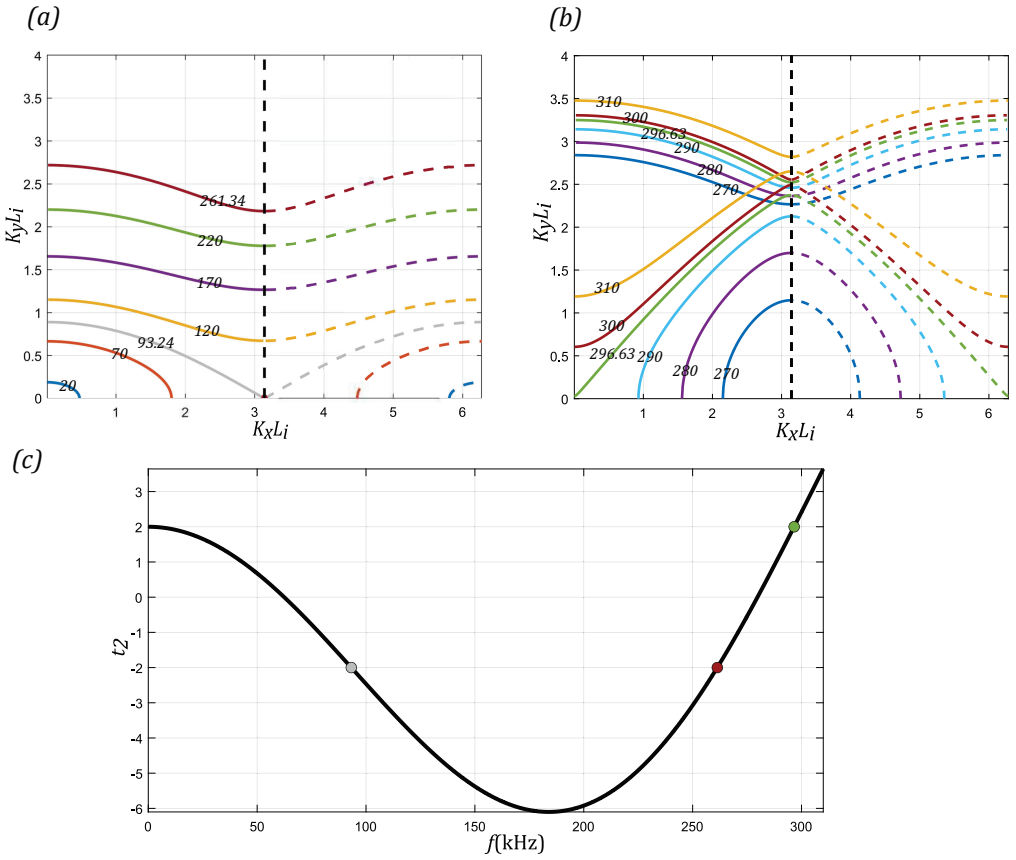

Figure 2: Laminate $\mathcal{F}_2$ combining PMMA and steel. (a), (b) Plots of real solutions of the dispersion equation in the graph K_yL_2 vs K_xL_2 for several given frequencies; in particular, (a) $f \in [20, 261.34]$ kHz, for each selected frequency and selected K_xL_2, either none or one mode of propagation is displayed, (b) $f \in [270, 296.63]$ kHz, for each selected frequency and selected K_xL_2, either one or two modes of propagation are displayed. (c) Plot of trace $t_2(f, 0)$, the grey point marks the upper limit of the first pass band, the red one that of the first stop band and the green one that of the second pass band.

also take place in the first Brillouin zone. Therefore, pure negative refraction is possible in principle only up to a well defined frequency for the problem at hand ($f = 296.63$ kHz in the analysed case), otherwise multiple waves are transmitted and the uniqueness is lost.

According to the definition introduced by Morini et al. (2019a), the two intervals $[0, 93.24]$ kHz and $[261.34, 296.63]$ kHz are *transition zones* (TZs) for the laminate $\mathcal{F}_2$; there, the number of real solutions of the dispersion equation depends on the frequency and increases of one unity reaching the upper limit of the zone (from 0 to 1 in the former interval, from 1 to 2 in the latter). For a frequency not sitting in a TZ, the number of solutions is fixed whatever the value of K_xL_i. It goes without saying that a threshold $\bar{K}_xL_i$ does exist for each frequency belonging to a TZ and the number of possible transmission modes depends on the comparison between $K_xL_i = K_0 \sin\theta^{\text{inc}} L_i$ (see eq. (6)) and $\bar{K}_xL_i$ (note that the comparison is given in dimensionless form, however the length L_i is irrelevant as it appears in both sides of the equation).

As values $\bar{K}_xL_i$ are read on the abscissa of the graph, where $K_y = 0$, the limits of the TZs can be

obtained from the analysis of the uniaxial problem in which the wave propagates orthogonally to the laminate, a condition that is mathematically governed by function $t_i(f,0)$. In the particular case of the laminate $\mathcal{F}_2$, the function $t_2(f,0)$ is sketched in Fig. 2(c) where it is not difficult to reach the following conclusion: TZs coincide to pass bands displayed by $t_2(f,0)$ ($t_i(f,0)$ in general), accordingly, their limits can be easily calculated. The three points sketched in the figure mark the limit of the first two pass bands (or TZs) and correspond exactly to 93.24, 261.34 and 296.63 kHz, respectively. For a generic laminate $\mathcal{F}_i$, we will refer to the three relevant frequencies as f_i^{1st} (upper limit of the first TZ), f_i^{2nd} (upper limit of the first stop band) and $\tilde{f}_i$ (upper limit of the second TZ).

Summarising, if the normalized wave number of incident wave $K_x L_i$ enters the second Brillouin zone, pure negative refraction could be obtained. The minimum frequency for wave number $K_x L_i > \pi$ is

$$f_i^{\min} = \frac{c_0}{2L_i} \tag{7}$$

(note that this value is for an incoming wave approaching the interface almost parallel to it, $\theta^{\mathrm{inc}} \to \pi/2$; for lower –and more likely– angles, the value of the minimum frequency increases). Thus, the conditions that must be *simultaneously fulfilled to achieve pure negative refraction* are:

(i) the frequency f of the incoming wave should satisfy $f_i^{\min} < f < \tilde{f}_i$ (here it is understood that the angle of incidence θ^{inc} is free);

(ii) if $f < f_i^{\mathrm{1st}}$, then it should be $K_x L_i > 2\pi - \bar{K}_x L_i$; if $f_i^{\mathrm{1st}} \leq f \leq f_i^{\mathrm{2nd}}$, $K_x L_i > \pi$ should be satisfied; if $f_i^{\mathrm{2nd}} < f < \tilde{f}_i$, it should be $K_x L_i > 2\pi - \bar{K}_x L_i$.

From Fig. 2, we may also conclude that *total reflection* of the shear wave occurs, for $f < f_i^{\mathrm{1st}}$, if $2\pi - \bar{K}_x L_i > K_x L_i > \bar{K}_x L_i$.

The number of transmitted modes across the interface depends on the comparison between K_x and $\bar{K}_x$: the former is determined by the frequency, the wave speed in substrate, the angle of incidence and the total length of the cell; the latter by function $t_i(f,0)$ (i.e. $\cos(\bar{K}_x L_i) = t_i(f,0)/2$), thus, the propagation of waves orthogonally to the laminate should be analysed further.

3 Canonical configurations for the laminate

3.1 Transmission matrix and canonical laminates

In this section, we analyse the transmission matrix for an anti-plane shear wave propagating orthogonally to the common direction of interfaces ($K_y = 0$) along a quasicrystalline-generated laminate with the goal of extending the concept of canonical configuration and canonical frequency proposed by Gei et al. (2020) in uniaxial wave propagation of periodic standard Fibonacci bars to the current type of microstructure.

If we set $K_y = 0$ into eq. (1), the equation specialises to $\mu\, \partial^2 u_z/\partial x^2 = \rho\, \partial^2 u_z/\partial t^2$, that is the one-dimensional Helmholtz equation governing harmonic longitudinal waves in bars whose solution is represented by eq. (2), duly specialised.

The properties of global transmission matrix for the cell provide the following recursion rule for traces t_i[2], i.e.

$$t_{i+1} = t_{i-1}t_i - t_{i-2} \quad (i \geq 2). \tag{8}$$

Through the new set of variables (Morini and Gei, 2018; Morini et al., 2019b)

$$\tilde{x}_i = t_{i+2},\ \tilde{y}_i = t_{i+1},\ \tilde{z}_i = t_i,$$

and its substitution into eq. (8), the following nonlinear map $\mathcal{T}$ setting out the evolution of t_i can be established

$$R_{i+1} = \mathcal{T}(R_i) = (\tilde{x}_i\tilde{y}_i - \tilde{z}_i, \tilde{x}_i, \tilde{y}_i), \tag{9}$$

where $R_i = (\tilde{x}_i, \tilde{y}_i, \tilde{z}_i)$ is a triplet whose entries are the traces of three consecutive indices.

The initial conditions to begin iteration of the map are

$$t_0 = 2\cos\left(2\pi f\frac{h_B}{c_B}\right), \quad t_1 = 2\cos\left(2\pi f\frac{h_A}{c_A}\right),$$

$$t_2 = 2\cos\left(2\pi f\frac{h_B}{c_B}\right)\cos\left(2\pi f\frac{h_A}{c_A}\right) - \beta\sin\left(2\pi f\frac{h_B}{c_B}\right)\sin\left(2\pi f\frac{h_A}{c_A}\right), \tag{10}$$

where coefficient β is the impedance mismatch

$$\beta = \frac{\mu_B c_A}{\mu_A c_B} + \frac{\mu_A c_B}{\mu_B c_A}.$$

The function of the frequency

$$I(f) = \tilde{x}_i^2 + \tilde{y}_i^2 + \tilde{z}_i^2 - \tilde{x}_i\tilde{y}_i\tilde{z}_i - 4 = (\beta^2 - 4)\sin^2\left(2\pi f\frac{h_A}{c_A}\right)\sin^2\left(2\pi f\frac{h_B}{c_B}\right) \tag{11}$$

is the (Kohmoto's) invariant of the sequence that is independent of index i. In the three-dimensional space described by the orthogonal cartesian system $O\tilde{x}\tilde{y}\tilde{z}$,

$$\tilde{x}^2 + \tilde{y}^2 + \tilde{z}^2 - \tilde{x}\tilde{y}\tilde{z} - 4 = I(f) \tag{12}$$

is the equation of a cubic, represented by a surface. Points R_i obtained by iterating map $\mathcal{T}$ belong to this surface for any given frequency f. The set of points generated through the iteration defines an orbit on the surface. Orbits can be either p-point periodic or non-periodic (Morini and Gei, 2018; Gei et al., 2020). In the former case, the discrete trajectory repeats itself after p applications of $\mathcal{T}$, i.e. $\mathcal{T}^p(R_i) = R_i$.

Surface (12) possesses six saddle points P_k $(k = 1, ..., 6)$, opposite in pairs, whose coordinates are $P_{1,4} = (0, 0, \pm\alpha_1)$, $P_{3,6} = (0, \mp\alpha_2, 0)$, $P_{2,5} = (\pm\alpha_3, 0, 0)$, where the top sign is associated with the lowest index and α_j $(j = 1, 2, 3)$ depend on frequency and value of the invariant. The saddle points are all part of a six-Point Periodic Orbit (PPO), which means that $\mathcal{T}^6(P_k) = P_k,\ \forall k$. Then, according to

[2]To ease the notation, in this section the quantity $t_i(f, 0)$ will be simply denoted by t_i.

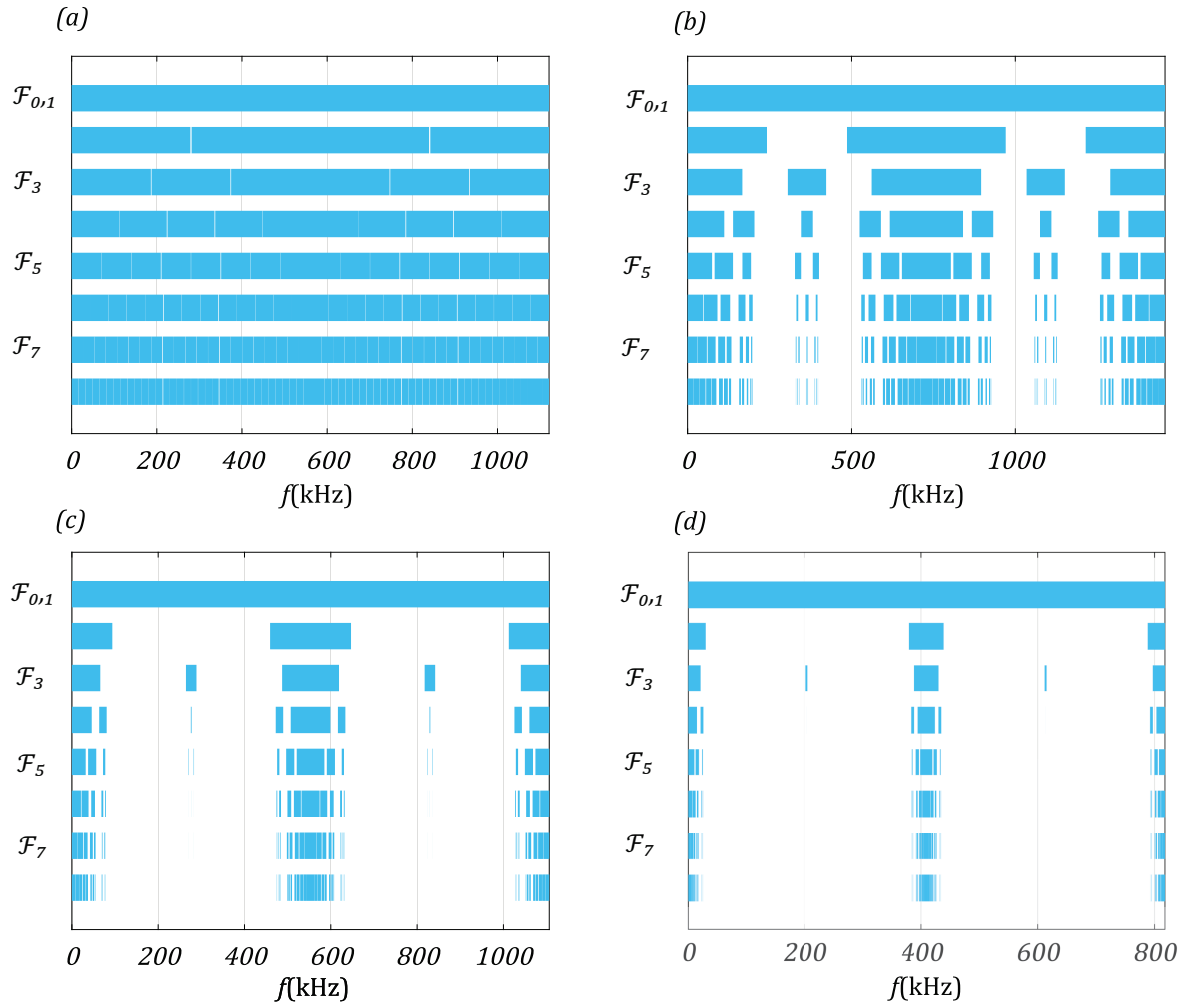

Figure 3: Stop- and pass-band layout for canonical Fibonacci laminates with four different impedance mismatches, but same canonical ratio $C^{(1)} = 1$. (a) Material A: iron, material B: copper, $\beta = 2.0002$; (b) A: steel, B: aluminium, $\beta = 3.351$; (c) A: PMMA, B: steel, $\beta = 13.520$; (d) A: steel, B: polyethylene, $\beta = 76.706$. In each plot, sequences $\mathcal{F}_0$ to $\mathcal{F}_8$ are displayed and the maximum value of the frequency is $4f_c$.

Gei et al. (2020), one of the following three conditions must be satisfied to achieve a 'closed' orbit on the surface

$$(1)\ \tilde{y}_0 = \tilde{z}_0 = 0, \quad (2)\ \tilde{x}_0 = \tilde{z}_0 = 0, \quad (3)\ \tilde{x}_0 = \tilde{y}_0 = 0. \tag{13}$$

The above three conditions imply that two out of three traces in eq. (10) vanish at some frequencies. The configurations for which this occurs are the *canonical configurations* and the frequencies are called the *canonical frequencies*. Substituting eqs. (10) in eqs. (13), the following relationships are derived:

$$C^{(1)} = \frac{1+2j}{1+2k}, \quad C^{(2)} = \frac{1+2j}{2q}, \quad C^{(3)} = \frac{2q}{1+2k} \quad (j,k,q \in \mathbb{N}), \tag{14}$$

respectively, where

$$C = \frac{c_A h_B}{c_B h_A} \tag{15}$$

is the *canonical ratio*. The superscript simply indicates the index, say (r), of the condition concerned in eq. (13), which defines the associated $r-$th Family ($r = 1, 2, 3$) of canonical configurations. In parallel with the problem of canonical rods, it is significant to notice that indices j, k and q are such that fractions on the right-hand sides of the equalities in eq. (14) must be in lowest terms. Family no. 1 corresponds to an odd/odd ratio, while odd/even and even/odd ratios are associated with Families no. 2 and 3, respectively. The *canonical frequencies* for each family can be written as $f_{cn}^{(r)} = f_c^{(r)}(1 + 2n)$ ($n \in \mathbb{N}$), where

$$f_c^{(1)} = \frac{c_A}{4h_A}(1 + 2k) = \frac{c_B}{4h_B}(1 + 2j), \quad f_c^{(2)} = \frac{c_A}{4h_A}2q = \frac{c_B}{4h_B}(1 + 2j),$$
$$f_c^{(3)} = \frac{c_A}{4h_A}(1 + 2k) = \frac{c_B}{4h_B}2q. \tag{16}$$

Note that $f_c^{(1)}$ and $f_c^{(2)}$ coincide. All conditions (14) force the functions $t_i(f, 0)$ for canonical laminates to be periodic, a property that leads to *periodic stop- and pass-band layouts*. The period of all traces corresponds to $4f_c$, while, due to the properties of traces themselves, the period of both the frequency spectra and the invariant $I(f)$ is $2f_c$.

Examples of sketch of pass bands and stop bands are displayed in Fig. 3 by assuming different materials A and B (listed in the caption) for sequences $\mathcal{F}_0$ to $\mathcal{F}_8$. For simplicity, $C^{(1)} = 1$ (Family no. 1) in all plots with total thickness for $L_2 = 0.0043$ m; thus, the thicknesses h_A and h_B depend on both canonical ratio and phase speed in the two materials. For instance, $h_A \approx 0.0014$ m and $h_B \approx 0.0029$ m for the combination PMMA (A) and steel (B) (see Tab. 1).

For all combination, the represented domain is $f \in [0, 4f_c]$. The pattern is clearly symmetric, actually there are two axes of symmetry at 1/4 and 3/4 of the domain that correspond to f_c and $3f_c$, respectively. The impedance mismatch β governs the density of stop bands: if $\beta = 2$, the laminate behaves as a homogeneous waveguide and the whole frequency range is in a pass band (see Fig. 3(a) where β is very close to 2). Conversely, for a high β, stop bands dominate the spectrum, that is the case displayed in Fig. 3(d).

The other important feature of the layout is the scaling of the self-similar structure of patterns in the vicinity of the canonical frequency. However, note that self similarity can also be noted at $f = 0$ and $f = 4f_c$. This is because at both $f = 0$ and $f = 4f_c$, a one–PPO occurs, i.e. $\mathcal{T}(R_i) = R_i$, or, in other words, $f = 0$ and $f = 4f_c$ are both *fixed points*. This example shows that other periodic orbits do exist on surface (12) at a canonical configuration. The general method to analyse scaling about a frequency where a periodic orbit occurs has been presented by Gei et al. (2020). For the goal of the paper, that is to exploit the concept of canonical configurations to predict the behaviour of the laminate in the problem of pure negative refraction, the focus should be on the first two pass bands at low frequencies as they coincide with the first two TZs for the laminate. Therefore, scaling at $f = 0$ plays an important role. For

this case, an alternative method to obtain the scaling parameter based on the invariant (11) is presented in the next Section.

In closing this part, it is worth remarking that for canonical ratios belonging to other families, considerations similar to those noted earlier for Family no. 1 can be proposed.

3.2 Scaling of traces at low frequencies

The layout of pass bands for a canonical configuration in the neighbourhood of $f = 0$ can be studied locally through the scaling of the observed self-similar structure. As the origin is a *fixed point*, by indicating with κ the scaling factor, it is expected that in this range the following approximations are valid, i.e.

$$t_{i+2}(f) \approx t_{i+1}(\kappa f) \approx t_i(\kappa^2 f). \tag{17}$$

To estimate κ, we can exploit the fact that $I(f)$ links three consecutive traces and its Maclaurin expansion is, at the lowest order,

$$I(f) \approx (\beta^2 - 4)C^2 \left(\frac{2\pi h_A}{c_A}\right)^4 f^4. \tag{18}$$

The next step is to observe that the Maclaurin expansion of any function $t_i(f)$ to the 2nd order can be represented as

$$t_i \approx 2 - \eta_i f^2, \tag{19}$$

where η_i is a coefficient that can be written in general as

$$\eta_i = [n_{i-1}^2 + n_{i-2}C(n_{i-2}C + n_{i-1}\beta)] \left(\frac{2\pi h_A}{c_A}\right)^2. \tag{20}$$

However, taking into account eqs. (17), the traces following t_i are

$$t_{i+1} \approx 2 - \eta_i \kappa^2 f^2, \quad t_{i+2} \approx 2 - \eta_i \kappa^4 f^2, \tag{21}$$

so that, in the neighbourhood of the origin, eq. $(11)_2$ takes the form

$$t_i(\kappa^2 f)^2 + t_i(\kappa f)^2 + t_i(f)^2 - t_i(\kappa^2 f)t_i(\kappa f)t_i(f) - 4 = (\beta^2 - 4)C^2 \left(\frac{2\pi h_A}{c_A}\right)^4 f^4. \tag{22}$$

A lengthy, but straightforward, calculation reveals that the l.h.s. of eq. (22) is a term in f^4 at lowest order, therefore an equation can be set up to provide the value of κ as a function of the other involved parameters. κ is strongly dependent on C, in the sense that for $C \to 0$, $\kappa \to \phi$, where ϕ is the 'golden ratio' $\phi = (\sqrt{5} + 1)/2$, independently of the other quantities. In any case, a careful evaluation of the scaling parameter has demonstrated that κ remains in the neighbourhood of ϕ independently of the index i assumed in eq. (22).

To describe the behaviour of traces at slightly higher frequencies, the approach presented so far can be extended by noticing that, to the fourth order, traces may be represented as

$$t_i \approx 2 - \eta_i f^2 + \zeta_i f^4, \tag{23}$$

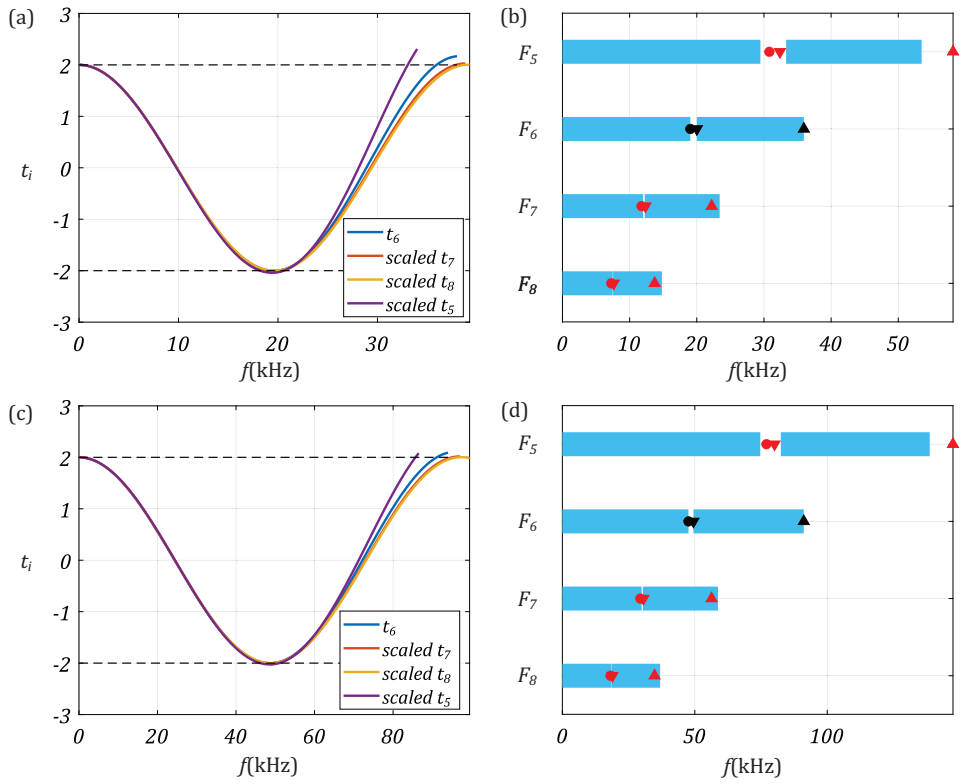

Figure 4: Scaling of traces at low frequencies in the vicinity of $f = 0$. Plot of traces for (a) $C = 1/5$, $\beta = 13.520$ and (c) $C = 1$, $\beta = 3.351$; in both plots, the adopted scaling factor is ϕ. (b), (c) Plot of the first two pass bands with prediction of their limits (indicated by red markers) obtained using the scaling factor ϕ starting from the exact limits of the pass bands for $\mathcal{F}_6$ (black markers).

where, similarly to η_i, coefficients ζ_i can also be written explicitly, and further expansion of the invariant provides

$$I(f) \approx (\beta^2 - 4)C^2 \left[\left(\frac{2\pi h_A}{c_A} \right)^4 f^4 - \frac{1 + C^2}{3} \left(\frac{2\pi h_A}{c_A} \right)^6 f^6 \right]. \tag{24}$$

Let us assume a second scaling parameter κ_1 governing the change in the fourth order terms of the two traces following t_i, i.e.

$$t_{i+1} \approx 2 - \eta_i \kappa^2 f^2 + \zeta_i \kappa_1^4 f^4, \quad t_{i+2} \approx 2 - \eta_i \kappa^4 f^2 + \zeta_i \kappa_1^8 f^4. \tag{25}$$

We can repeat the procedure followed before and obtain an equation in f^6 in both κ and κ_1. Coupling this with the equation only in κ obtained previously, it turns out that also κ_1 depends, in general, on the parameters of the problem and, similarly to κ, obeys the limit $\kappa_1 \to \phi$ for $C \to 0$. This confirms once again that the golden ratio governs scaling at low frequencies.

Fig. 4 displays how the scaling works for two material combinations: PMMA/steel for Figs. 4(a), (b) and steel/aluminium for Figs. 4(c), (d). In both parts (a) and (c), a set of 'scaled' traces in the neighbourhood of the origin are drawn; in particular, in both panels the horizonal domain is that of

t_6, while functions t_5, t_7 and t_8 are scaled accordingly by adopting ϕ as a factor. Those plots show that when $t_i \approx -2$, the upper limit of the first pass band (i.e. frequency $f_i^{1\mathrm{st}}$) and the lower limit of the second one (i.e. frequency $f_i^{2\mathrm{nd}}$) are captured very well by the theory. A slightly worst match is obtained for the upper limit of the second pass band (i.e. frequency $\tilde{f}_i$), but this issue can be explained well by the fact that the involved frequencies are relatively far from the origin and the scaling is much more effective at relatively high index i.

In parts (b), (d) of the same figure, the first two pass bands for the traces represented alongside are sketched together with red markers indicating prediction of the their limits obtained by scaling up or down the corresponding exact values for $\mathcal{F}_6$ (black markers). The two plots once again demonstrate that scaling is an effective tool to control the breadth of the first two pass bands. For the point of view of the laminate as an elastic device, the quantitative estimate of the scaling of the self similar pattern of TZs at low frequencies may help to select the index of the most suitable elementary cell to achieve pure negative refraction when coupled to an isotropic substrate.

4 Analysis of the boundaries of the first two transition zones at low frequencies

In closing the previous section, we have recalled that knowledge of the first two TZs at low frequencies (or, alternatively, of the three frequencies $f_i^{1\mathrm{st}}$, $f_i^{2\mathrm{nd}}$ and $\tilde{f}_i$) is the key information to assess if pure negative refraction may occur for a given substrate-laminate combination. We intend to continue the investigation into the limits of TZs and the role of canonical frequency by briefly dealing with three issues.

The first one to address is to verify how the change of the materials of the two phases A and B modifies the value of the three frequencies at fixed canonical ratio C. The quest arises from the fact that it is clear from Fig. 3 that (i) an increase of the impedance mismatch β promotes the presence of stop bands to the detriment of pass bands and (ii) the number of TZs within the interval $[0, f_\mathrm{c}]$ for same canonical ratio and index i is independent of β (this is why we notice that in all four panels of Fig. 3 the second TZ for cell $\mathcal{F}_2$ (resp. $\mathcal{F}_3$) is always centred at $2f_\mathrm{c}$ (resp. f_c)). Thus, the values of the ratios between each of the three relevant frequencies and the canonical one (i.e. $f_i^{1\mathrm{st}}/f_\mathrm{c}$, $f_i^{2\mathrm{nd}}/f_\mathrm{c}$ and $\tilde{f}_i/f_\mathrm{c}$) can be employed to evaluate the influence of parameter β on the limits of the first two TZs. To this end, Fig. 5 reports the corresponding plots for $C = 1$. The numerical results have been obtained by changing the thicknesses h_A and h_B to accommodate the change in material properties (cf. eq. (15)). In the figure, it may be observed that at an increasing β, $f_i^{1\mathrm{st}}$ and $\tilde{f}_i$ decrease w.r.t. f_c, except for cell $\mathcal{F}_2$ (see Fig. 5(a) and (c)); conversely, $f_i^{2\mathrm{nd}}/f_\mathrm{c}$ increases for $\mathcal{F}_2$ and $\mathcal{F}_3$, reaching $2f_c$ and f_c in the limit of infinite contrast, respectively; for higher indices of the sequence, the same ratio decreases. A behaviour similar to the latter is also followed by $\tilde{f}_i/f_\mathrm{c}$, that reaches the values 2 and 1, respectively, for $\beta \to \infty$.

Second, we wonder: what happens if the two phases, A and B, swap? As β does not change, the spectrum is the same, but scaled according to the change of value of f_c brought about by the swap (see

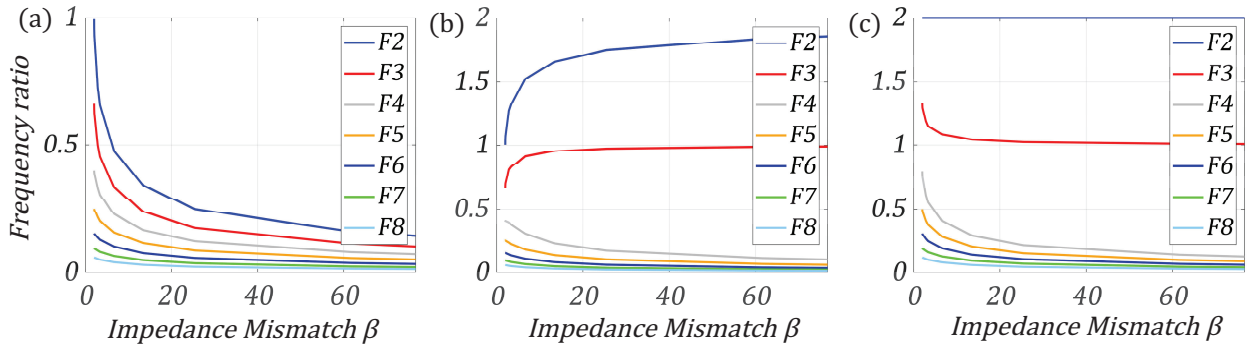

Figure 5: Plot of functions (a) $f_i^{\mathrm{1st}}/f_{\mathrm{c}}$, (b) $f_i^{\mathrm{2nd}}/f_{\mathrm{c}}$ and (c) $\tilde{f}_i/f_{\mathrm{c}}$ as a function of impedance mismatch β (canonical ratio $C = 1$).

eq. (16)). As a consequence, the three frequencies are in the same proportion with f_{c}.

The third observation stems from the fact that in eq. (7) the speed c_0 is a property of the substrate, then the length L_i in the same equation could be selected to tune the frequency. In particular, with the aim of widening the possibility of pure negative refraction, it could be useful to maximise quantity $L_i\tilde{f}_i$. As the total length of the cell is $L_i = n_i^{(A)}h_A + n_i^{(B)}h_B$ (see Sect. 2.1), then h_B can be solved from the definition of canonical ratio, eq. (15), yielding $h_B = Cc_Bh_A/c_A$. Therefore, with the help of eqs. (14) and (16), L_if_{c} can be calculated for the three Families of canonical laminates as follows:

$$L_if_{\mathrm{c}}^{(1)} = \frac{1}{4}[(1+2k)n_i^{(A)}c_A + (1+2j)n_i^{(B)}c_B],$$

$$L_if_{\mathrm{c}}^{(2)} = \frac{1}{4}[2qn_i^{(A)}c_A + (1+2j)n_i^{(B)}c_B], \quad L_if_{\mathrm{c}}^{(3)} = \frac{1}{4}[(1+2k)n_i^{(A)}c_A + 2qn_i^{(B)}c_B], \tag{26}$$

respectively, where note that indices $j,\ k,\ q$ are those defining the canonical ratio in eq. (14). Thus, the two materials A and B can be selected in order to maximise the value obtained from the corresponding equation among the three listed in (26); for instance, $L_3f_3^{\mathrm{1st}}$, $L_3f_3^{\mathrm{2nd}}$ and $L_3\tilde{f}_3$ are higher for the combination A: steel, B: PMMA, than the opposite one with the same canonical ratio. Therefore, the canonical frequency can be used as a key quantity to investigate the influence of impedance mismatch in maximising the relevant frequencies for assessing whether or not pure negative refraction may take place.

We close this section by recalling that our focus was mainly placed on *pure* negative refraction and then, for the classification presented in Subsect. 2.2, on the first two TZs of the spectrum. However, for a canonical laminate the layout of the TZs is symmetric and periodic, therefore this feature can be exploited at high frequency to determine the number of transmitted waves (either positive or negative refracted) by linking the frequency to the corresponding one in the first period.

5 Conclusions

A method to accomplish pure negative refraction for harmonic elastic anti-plane shear dynamics is wave transmission across an interface between a substrate and a composite laminate whose lamination direction is orthogonal to the interface. Previous studies have shown that the goal is achievable if the frequency of the impinging wave is compatible with propagation of the refracted wave within the second Brillouin zone of the laminate (this has been reviewed in the first Section of the manuscript). Therefore, the study of the dispersion properties of the composite is a fundamental task to be carried out in detail. The control of those properties is particularly easy for a special class of laminates, called *canonical*, that can be studied by considering sets of elementary cells generated by a quasicrystalline sequence (the Fibonacci sequence in this case). For waves propagating orthogonally to the lamination direction, canonical laminates display a periodic stop- and pass-band layout, the periodicity being governed by a special frequency called *canonical* frequency. The key features leading to the definition of such special configurations are (i) the recursive relationship existing between three consecutive traces of transmission matrices, (ii) the existence of an invariant function and (iii) the nonlinear trace map that can be written from the recursive rule: the canonical configurations correspond to periodic orbits of the trace map and this takes place at well-defined frequencies, namely, the canonical frequencies. The theory shows that there are three families of canonical laminates.

For the problem of pure negative refraction, the focus is on the first two pass bands of the spectrum that possess the same limits of the first two transition zones at low frequencies for the laminate if we consider wave propagation in any direction. The self-similar pattern displayed by them at increasing index of the sequence can be quantitatively described through a scaling factor that can be estimated by performing Maclaurin expansions of trace functions and substituting them in the expression of the invariant. Through this parameter, the breadths of the two transition zones can be predicted by scaling backward and/or forward the corresponding values of a given configuration taken as a reference. It is also shown how the impedance mismatch of the laminate affects the limits of the transition zones at constant canonical ratio and how to modify the dispersive properties of the elementary cell by changing its total length.

The concept of canonical laminate sheds a new light on the way to achieve pure negative refraction in periodic elastic composites as it helps to control the relevant frequencies which govern the phenomenon. It is envisaged that the methodology set out in this paper could be extended to other types of periodic waveguides composed of micro-architected materials.

Acknowledgments. Z.C. acknowledges support from China Scholarship Council (Grant No. CSC201908500111). M.G. is grateful to the support provided by University of Trieste through grant FRA2021 'NEO-PHONON'.

References

Brun, M., Guenneau, S., Movchan, A.B., Bigoni, D., 2010. Dynamics of structural interfaces: filtering and focussing effects for elastic waves. J. Mech. Phys. Solids 58, 1212–1224.

Carta, G., Jones, I.S., Movchan, N.V., Movchan, A.B., Nieves, M.J., 2017. "Deflecting elastic prism" and unidirectional localisation for waves in chiral elastic systems. Sci. Rep. 7, 26.

Colquitt, D.J., Jones, I.S., Movchan, N.V., Movchan, A.B., Brun, M., McPhedran, R.C., 2013. Making waves round a structured cloak: lattices, negative refraction and fringes. Proc. R. Soc. A 469, 20130218.

Farhat, M., Guenneau, S., Enoch, S., Movchan, A.B., 2009. Negative refraction, surface modes, and superlensing effect via homogenization near resonances for a finite array of split-ring resonators. Phys. Rev. E 80, 046309.

Farhat, M., Guenneau, S., Enoch, S., Movchan, A.B., Petursson, G.G., 2010. Focussing bending waves via negative refraction in perforated thin plates. Appl. Phys. Lett. 96, 081909.

Gei, M., Chen, Z., Bosi, F., Morini, L., 2020. Phononic canonical quasicrystalline waveguides. Appl. Phys. Lett. 116, 241903.

Jones, I.S., Movchan, A.B., Gei, M., 2011. Waves and damage in structured solids with multi-scale resonators. Proc. R. Soc. A 467, 964–984.

Lekner, J., 1994. Light in periodically stratified media. J. Opt. Soc. Am. A 11, 2892–2899.

Morini, L., Eyzat, Y., Gei, M., 2019a. Negative refraction in quasicrystalline multilayered metamaterials. J. Mech. Phys. Solids 124, 282–298.

Morini, L., Gei, M., 2018. Waves in one-dimensional quasicrystalline structures: dynamical trace mapping, scaling and self-similarity of the spectrum. J. Mech. Phys. Solids 119, 83–103.

Morini, L., Tetik, Z.G., Shmuel, G., Gei, M., 2019b. On the universality of the frequency spectrum and band-gap optimization of quasicrystalline-generated structure rods. Phil. Trans. R. Soc. A 378, 20190240.

Nemat-Nasser, S., 2015. Anti-plane shear waves in periodic elastic composites: band structure and anomalous wave refraction. Proc. R. Soc. A 471, 20150152.

Poddubny, A.N., Ivchenko, E.L., 2010. Photonic quasicrystalline and aperiodic structures. Physica E 43, 1871–1895.

Srivastava, A., 2016. Metamaterial properties of periodic laminates. J. Mech. Phys. Solids 96, 252–263.

Srivastava, A., Nemat-Nasser, S., 2014. On the limit and applicability of dynamic homogenization. Wave motion 51, 1045–1054.

Srivastava, A., Willis, J.R., 2017. Evanescent wave boundary layers in metamaterials and sidestepping them through a variational approach. Proc. R. Soc. A 473, 20160765.

Tallarico, D., Movchan, N.V., Movchan, A.B., Colquitt, D.J., 2017. Tilted resonators in a triangular elastic lattice: Chirality, Bloch waves and negative refraction. J. Mech. Phys. Solids 103, 236–256.

Willis, J.R., 2016. Negative refraction in a laminate. J. Mech. Phys. Solids 97, 10–18.